Jpn. J. Appl. Phys. Vol. 38 (1999) pp. 5898–5904
Part 1, No. 10, October 1999

Femtosecond Pulse Shaping with Twisted-Nematic Liquid-Crystal Spatial-Light Modulators

Toshiaki HATTORI*, Kouhei KABUKI, Yoshitsugu KAWASHIMA, Masahiro DAIKOKU and Hiroki NAKATSUKA
Institute of Applied Physics, University of Tsukuba, Tennodai, Tsukuba, Ibaraki 305-8573, Japan

(Received June 14, 1999; accepted for publication July 28, 1999)

Shaping of 16 fs optical pulses using a twisted-nematic (TN) liquid-crystal spatial-light modulator (SLM) was conducted. The properties of TN SLMs were characterized theoretically and experimentally, and the relevant mode extraction method was developed for the SLM mask pattern design using a simulated annealing algorithm. Phase-sensitive pulse shaping using a TN SLM was performed and the shaped waveforms were observed by measuring the interferometric intensity cross-correlation with unshaped pulses.

KEYWORDS: pulse shaping, femtosecond, liquid crystal, spatial light modulator

1. Introduction

Recently, much attention has been paid to the development of a technique for the generation of temporally shaped femtosecond optical pulses.[1–6] Thus far, pulse shaping using a grating-lens apparatus with a liquid-crystal spatial-light modulator (SLM) has been proven to be a powerful method for synthesizing complex femtosecond optical waveforms. One-dimensional (1-D) SLMs which can independently control the amplitude and the phase of the transmitted light have been specially designed for pulse shaping, and are now commercially available. On the other hand, liquid-crystal SLMs for commercial use are being developed very rapidly, and two-dimensional (2-D) SLMs with very large pixel numbers are available at a low cost. The advantages of using these SLMs in the pulse-shaping apparatus are as follows: i) They have a very large number of pixels (a maximum of 1280×1024 pixels is available at present, compared with 128 pixels in conventional 1-D SLMs). This corresponds to a much larger complexity, or a much longer time window, available for the waveforms of the shaped pulses. ii) The possibility of 2-D independent control of the modulation allows a new degree of freedom in pulse shaping. The new dimension can be used for spatial or wavevector shaping of the pulse.[6]

There is also a potential disadvantage to using commercial 2-D SLMs. Since they most often have a twisted-nematic (TN) structure, the amplitude and the phase of the transmitted light are coupled in a specific manner. This makes the design procedure of the SLM modulation pattern less straightforward than that with a mask which can give arbitrary amplitude and phase. In this study, we focused on pulse shaping with TN SLMs in the time domain, and investigated the potential of the technique.

2. Experimental Method

The design of the pulse shaping apparatus is shown in Fig. 1. It is similar to those used previously for the shaping of 20 fs or 13 fs pulses by other groups.[1,3] It consists of one pair of 600 line/mm gratings, two spherical concave mirrors with a focal length $f = 200$ mm, and a liquid-crystal SLM. The diffraction angle of the beams on the grating on the input side was $\theta_d = 4.3°$. These components were placed on a horizontal plane.

The SLM used was a 1.3 inch active-matrix thin-film-transistor TN liquid-crystal panel module (EPSON, P13VM215) with 640 (horizontal) $\times$ 480 (vertical) pixels. This module has been commercialized for use in liquid-crystal projectors, and can be controlled by a personal computer equipped with a Super Video Graphics Array (SVGA) video card, which enables 256-level independent control of the voltage applied on each pixel of the SLM. The pitch of the pixels was 42 μm/pixel for both horizontal and vertical directions. The light, which was frequency-dispersed in the horizontal direction, was focused to a line with a vertical width of a few pixels on the SLM. If the focusing lens is replaced with a cylindrical lens, the light is not focused in the vertical direction, and spatiotemporal pulse shaping can be performed by making the vertical dimension correspond to the real space.[6]

The light incident to the pulse-shaping apparatus had vertical polarization, the light transmitted through the SLM passed a polarizer which was attached to the SLM, and only the light with the same polarization direction was sent to the waveform measurement setup. In commercial video instruments, liquid-crystal SLMs are most often used in the normally white mode, in which the SLMs are placed between crossed polarizers, and transmitted light has polarization perpendicular to the incident polarization. In the present study, however, we observed the transmitted light with polarization parallel to that of the incident light. In this configuration, we can eliminate structures in the spectrum of the diffraction efficiency of the gratings, which are apparent only with *p*-polarized light.

In a TN structure, a thin film of nematic liquid-crystal material is contained between parallel glass plates. The orientation of the liquid-crystal molecules lies in the plane parallel to

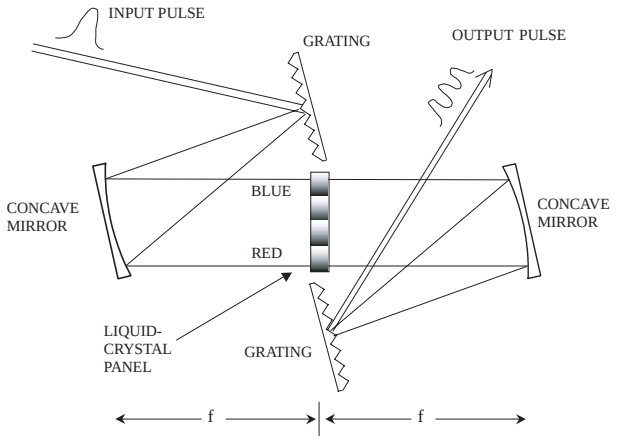

Fig. 1. Schematic of the setup of the pulse-shaping apparatus used in the present study.

*E-mail address: hattori@bk.tsukuba.ac.jp

the panel surfaces when no voltage is applied, and is gradually twisted from one surface to the other by an angle (twist angle) of around 90°. When voltage is applied to the panel, the molecules tend to realign parallel to the applied electric field. By changing the applied voltage level, the degree of alignment can be controlled. The material has birefringence to the light incident normally to the surface, and the axis of the birefringence is twisted from one surface to the other along with the twist of the molecules. The refractive index for light with electric field perpendicular to the molecular axis, n_o, is independent of the alignment of the molecules, and the refractive index for light with magnetic field perpendicular to the molecular axis, n_e, is dependent on the molecular alignment. The difference between these indices, Δn, is thus dependent on the applied voltage.

The polarization properties of light transmitted through a TN liquid-crystal structure in the normally white mode was studied by Gooch and Tarry.[7] The amplitude and the phase of the transmitted light in the present polarization combination can be derived in a similar manner. The resulted complex transmission coefficient is[6]

$$\mathcal{T} = \frac{\sin\left(\frac{\pi}{2}\sqrt{1+u^2}\right)}{\sqrt{1+u^2}} \exp\left(-\frac{i\pi u}{2}\right). \quad (1)$$

Here, u is a parameter proportional to the birefringence of the liquid-crystal medium, and is defined as

$$u = \pi l \Delta n / \theta \lambda, \quad (2)$$

where l is the thickness of the liquid-crystal cell, $\theta = \pi/2$ is the twist angle, and λ is the wavelength of the light. It is expected that u can be changed from 0 (complete transmission) at the maximum voltage level to $\sqrt{3}$ (no transmission) at the minimum voltage by changing the voltage applied to the liquid crystal. The twist angle θ was assumed to be $\pi/2$ in the derivation of eq. (1). This expression was obtained by substituting $\theta = \pi/2$ in the more general expression for the transmission coefficient of light with input polarization parallel to one of the birefringence axes and output polarization perpendicular to the same axis. Since the axis is twisted along the transmision of light through the material, the general expression for the transmission coefficient with an arbitrary twist angle for the same input and output polarization cannot be derived from this, and is much more complicated and dependent on the direction of the birefringence axis. The relationship between the transmittance, which is the squared magnitude of the amplitude, and the phase of the transmitted light based on eq. (1) is plotted in Fig. 2. It is seen from the figure that the amplitude and the phase are completely coupled to each other, and that the maximum phase change that the SLM can generate is $\sqrt{3}\pi/2$.

The light source used in the pulse-shaping experiments was a home-built Kerr-lens mode-locked Ti:sapphire laser. The laser cavity was dispersion-compensated by an intracavity silica prism pair. The cavity configuration was based on the design reported by Asaki *et al.*,[8] and pumped by an intracavity frequency-doubled Nd:YVO_4 laser with an output power of 5 W (Spectra Physics, Millennia V). The Ti:sapphire crystal had a path length of 4.5 mm. The pulse width, the wavelength, the average power, and the repetition rate of the output pulses were 16 fs, 822 nm, 600 mW, and 83 MHz, respectively.

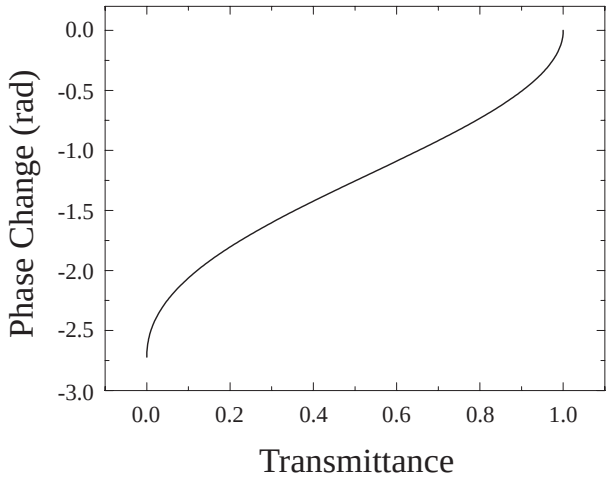

Fig. 2. Relationship between the transmittance and the phase change of the light transmitted through a TN liquid- crystal SLM. The calculation assumes a liquid-crystal twist angle of 90°.

The frequency dispersion of the light per pixel on the SLM was[4]

$$\Delta\nu = \frac{cd\Delta x_{\text{pixel}} \cos\theta_d}{f\lambda^2} = 0.155\,\text{THz/pixel}, \quad (3)$$

where c is the speed of light, d is the grating period, and $\Delta x_{\text{pixel}} = 42\,\mu$m is the SLM pixel pitch. Sixteen fs pulses with sech^2 temporal intensity profile have a full-width at half maximum spectral width of 19.7 THz, which corresponds to 127 pixels.

3. Mask Pattern Design

The coupling of the amplitude and the phase of the light transmitted through the SLM, as shown in Fig. 2, can impose some limitations in the types of waveforms which pulse shapers with this SLM can generate. Limitations notwithstanding, the large number of pixels on the present SLM nevertheless allows sufficient freedom for the generation of many practical and useful waveforms.

A simulated-annealing (SA) computer program[9] which incorporates the amplitude-phase relation expressed in eq. (1) was written for the design of the SLM mask pattern. We newly introduced the relevant mode extraction (RME) method in the SA calculation, which is discussed below in detail. The SA algorithm has been used previously to design mask patterns of phase-only SLMs,[2,3] and has succeeded in generating pulse trains which consist of pulses the shape of which is the same as that of the incident pulse. These methods, however, met with limited success in generating waveforms with features that deviated significantly from that of the input pulse on the timescale of the input pulse width. In the present study, therefore, we selected target pulses which consist of replicas of the unshaped pulse with the spacings and the complex amplitude ratios specified. The waveforms can be expressed as

$$E_{\text{target}}(t) = e(t) \otimes \sum_{k=1}^{N} A_k\,\delta(t - T_k). \quad (4)$$

Here, $e(t)$ is the field profile of an unshaped pulse, N is the number of constituent pulses, A_k is the complex amplitude of each pulse, T_k is the temporal position of each pulse, and $\otimes$ is the convolution operator. The positions of all pulses,

T_k, are limited in the positive (or negative) time region due to the limited modulation capability of the present SLM, as discussed below.

First, in Fig. 3 we show a simple example of a simulated waveform obtained by SA calculation, which illustrates the types of waveforms which TN SLMs can generate. In this example, the calculation searched for an SLM mask pattern which generates as high intensity at $T_1 = 126$ fs and as low intensity at other positive times as possible. The input pulse was assumed to be a 16 fs sech^2 pulse. The peak intensity of the input pulse was normalized to unity. The resulted waveform has a high peak at 126 fs, as expected. There remains, however, a peak at time zero with a comparable intensity, and several small peaks are also apparent at the negative times of $-T_1$, $-2T_1$, $-3T_1$, and $-4T_1$. The persistence of the input pulse at time zero is due to the limited possible phase change, as seen in Fig. 2. The appearance of peaks at negative times is due to the coupling of the amplitude and the phase. In the positive time region, however, a single large pulse at $t = T_1$ is observed with the exception of very small peaks at $t = 3T_1$ and $4T_1$. These are the general features observed in waveforms which the present TN SLMs can generate. Since the temporal position of the pulse T_1 can be made as large as several picoseconds in the present experimental setup, we have a time window sufficiently long in the positive time region for conducting many types of useful time-resolved measurements with the shaped pulses. Because the shaped pulse at T_1 has a peak intensity comparable to the remaining input pulse at time zero, experiments using the two-pulse sequence can also be conceived using this type of waveform. The phase of the shaped pulse at T_1 can be arbitrarily specified, as described in §4.

We now describe the procedure required for the calculation of shaped waveforms, as shown in Fig. 3. The input field spectrum used in the calculation had a Gaussian shape with a width slightly larger than that of the experimentally used input pulse. This is to guarantee clean mask patterns even in the wing regions, where the experimental spectrum does not have significant amplitudes. The spectrum was then multiplied by the complex transmission coefficient of the SLM expressed in eq. (1). The temporal waveform $E_{\text{guess}}(t)$ was obtained by an inverse Fourier transform of the spectrum. The purpose of the calculation was to obtain an SLM mask pattern which maximizes the peak intensity at $t = T_1$ and minimizes the intensity in the baseline region, i.e., in the positive time region except for very short times, where the input pulse remains, and around T_1. The cost function used has the form:

$$J[u(\omega)] = W_{\text{base}} \max\{|E_{\text{guess}}(t)|^2\} - W_{\text{pulse}}|E_{\text{guess}}(T_1)|^2. \tag{5}$$

Here, max{ } is the maximum value of the argument in the baseline region, as described above, and W_{base} and W_{pulse} are the weight factors. By using the SA algorithm,[9] a mask pattern which minimizes the cost function was obtained.

The advantages of the use of cost functions of this form over those previously used in the literature[2,3] are as follows: i) The largest possible peak height is obtained automatically. In previous studies,[2,3] the largest possible pulse height was found only after many trials of the SA calculations with different target pulse heights. ii) The relative weights of the contributions of the peak height and the baseline to the cost function can be tuned. The relative importance of the two contributions is dependent on the types of experiments in which the shaped pulses are used. Some types of experiments require very clean baselines. Only a large peak height is required in other types of experiments. Therefore, the ability to tune the relative weight in the cost function is useful in obtaining the pulse shape most appropriate for the experiments in which the shaped pulses are used.

The obtained mask pattern was used to calculate the waveform of the output pulse shaped from the actual 16 fs sech^2 pulse. The waveform shown in Fig. 3 was obtained by following these procedures, and the obtained mask pattern which generates this waveform is shown in Fig. 4.

The cost function above is only applicable for a waveform which consists of a single pulse. To obtain a multiple pulse sequence, we developed the RME method. Here, the targets are waveforms which consist of N pulses at T_k ($k = 1 \ldots N$) in the positive time region with target relative intensities P_k ($k = 1 \ldots N$) specified. Normalized target intensities are defined as

$$p_k = P_k / \sqrt{\sum_{k=1}^{N} P_k^2}. \tag{6}$$

Let the intensities of the temporary calculated waveforms at the target temporal positions of pulses T_k be

$$I_k = |E_{\text{guess}}(T_k)|^2. \tag{7}$$

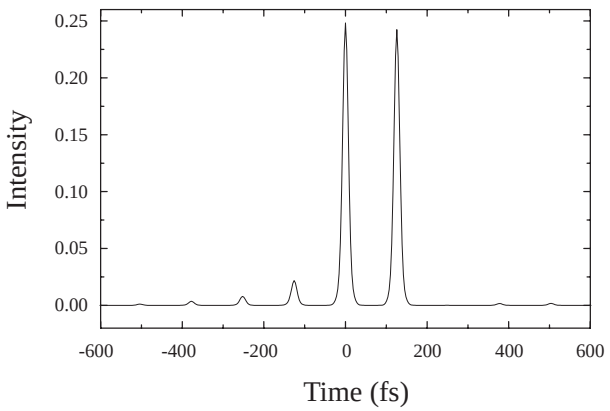

Fig. 3. Simulated waveform with a single pulse at 126 fs in the positive time region. The peak intensity of the input pulse is normalized to unity.

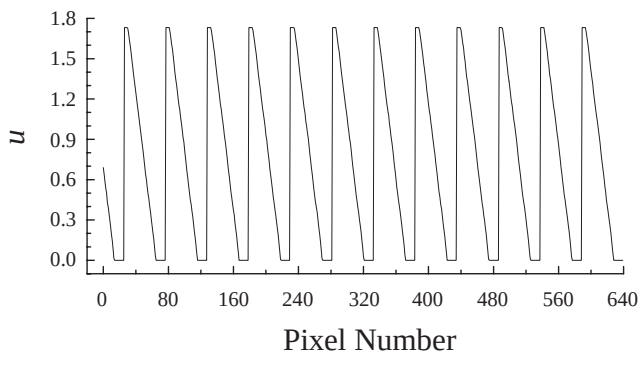

Fig. 4. SLM mask pattern which generates the waveform shown in Fig. 3 obtained by a simulated annealing calculation. The vertical axis shows the birefringence parameter u of each pixel. The amplitude and the phase of the transmitted light are given in eq. (1) as a function of u.

I_k ($k = 1 \ldots N$) span an N-dimensional space. The purpose of the calculation here is to maximize the relevant normal mode amplitude:

$$q_0 = \sum_{k=1}^{N} p_k I_k, \tag{8}$$

and simultaneously suppress the amplitudes of all the normal modes which span the $(N-1)$-dimensional space orthogonal to the relevant mode; q_k ($k = 1 \ldots N-1$). Using the summation rule:

$$\sum_{k=0}^{N-1} q_k^2 = \sum_{k=1}^{N} I_k^2, \tag{9}$$

the cost function in the SA calculation was set as

$$J[u(\omega)] = W_{\text{base}} \max\{|E_{\text{guess}}(t)|^4\} - W_{\text{pulse}} \left[q_0^2 - S \left(\sum_{k=1}^{N} I_k^2 - q_0^2 \right) \right]. \tag{10}$$

Here, S is a factor which controls the degree of suppression of the amplitudes of the modes which are orthogonal to the relevant modes.

Some examples of waveforms calculated using this cost function are shown in Fig. 5. The target waveform of trace (a) consists of two pulses at 126 and 220.5 fs with the same peak intensity. The target waveforms of (b) and (c) consist of five pulses at 126, 220.5, 315, 409.5, and 504 fs with peak intensity ratios of (b) 1 : 1 : 1 : 1 : 1 and (c) 1 : 2 : 3 : 2 : 1. The peak intensity of the input pulses is normalized to unity. The corresponding mask patterns are shown in Fig. 6. It is clearly seen that multiple pulse sequences with intensity ratios close to those designed are obtained, and that the waveforms have a very clean baseline in the positive time region. It is also found that a relatively large portion (16–23%) of the incident pulse energy is converted to waveforms in the target time window.

In the examples described above, only the intensity profiles were designed, and the phase of the field was not specified. The RME method, however, can also be applied to phase-sensitive shaping, as described in §4.

It should be noted that the application of the RME method is not limited to the shaping of waveforms expressed in eq. (4). Mask patterns which generate waveforms consisting of pulses with temporal profiles different from that of the unshaped pulse can also be designed using the RME method. In this case, the intensity of the waveform at each discrete time replaces I_k in eq. (7). The intensity of the obtained shaped pulse is maximized automatically in the same manner as in the case described above.

4. Experimental Results

In order to observe not only the amplitude but also the phase profile of the shaped waveforms, we performed collinear interferometric intensity cross-correlation measurements using the setup shown in Fig. 7. The femtosecond

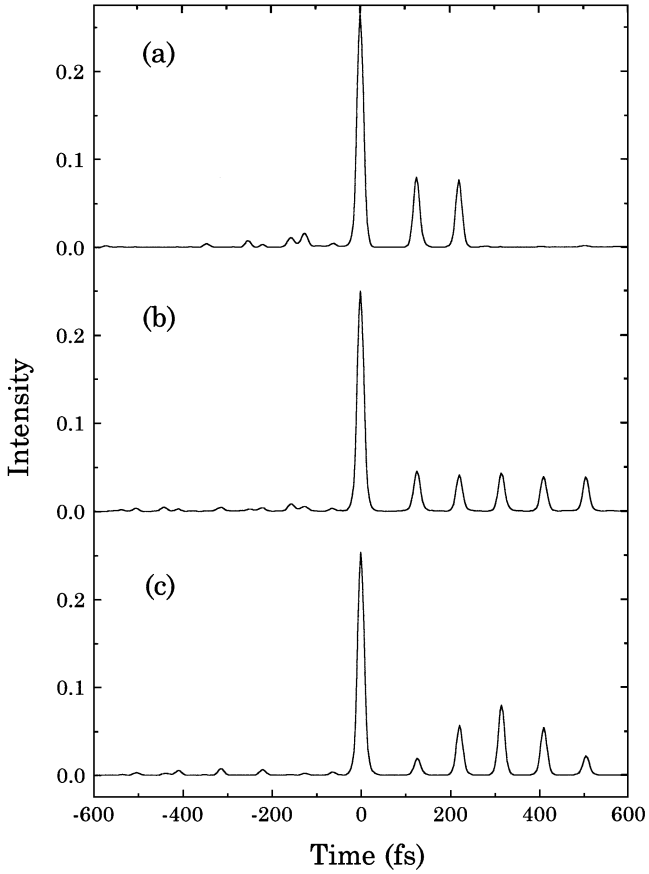

Fig. 5. Waveforms calculated using the relevant mode extraction method. The peak intensity of the input pulse is normalized to unity. The temporal positions and the relative intensities of the constituent pulses of the target waveforms are as follows: (a) 126 fs and 220.5 fs, 1 : 1, (b) 126 fs, 220.5 fs, 315 fs, 409.5 fs, and 504 fs, 1 : 1 : 1 : 1 : 1, (c) 126 fs, 220.5 fs, 315 fs, 409.5 fs, and 504 fs, 1 : 2 : 3 : 2 : 1.

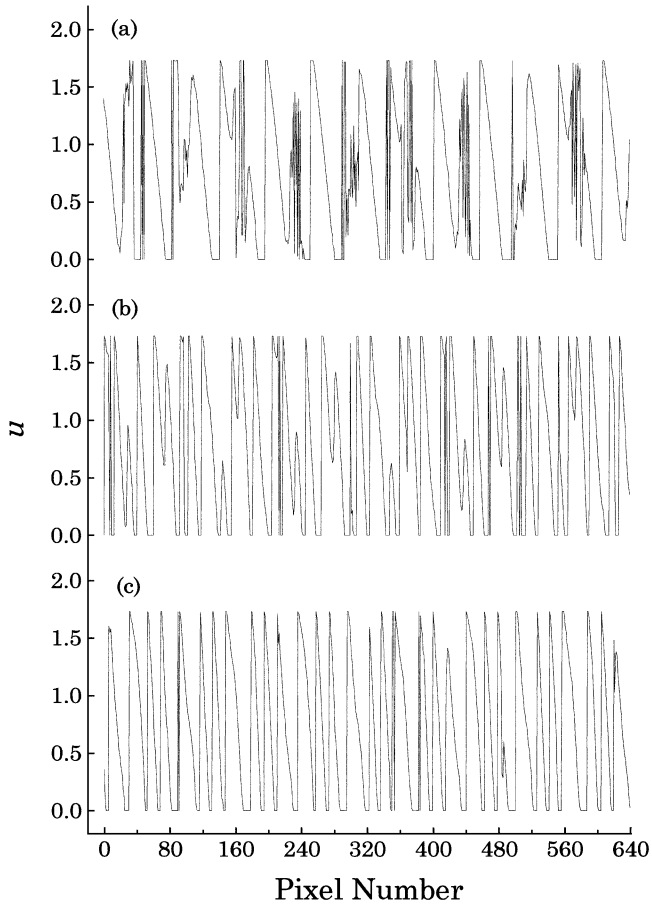

Fig. 6. SLM mask patterns which generate the waveforms shown in Fig. 5. Patterns (a), (b), and (c) correspond to waveforms (a), (b), and (c) in Fig. 5.

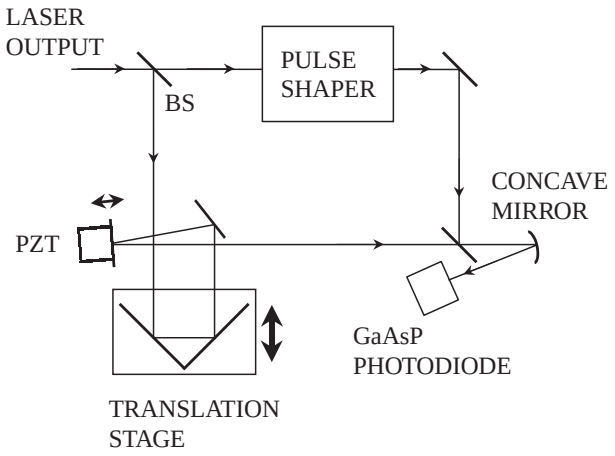

Fig. 7. Schematic of the experimental setup for the interferometric measurement of the intensity cross-correlation of the shaped pulse and the unshaped pulse. BS: beam splitter, PZT: piezoelectric actuator.

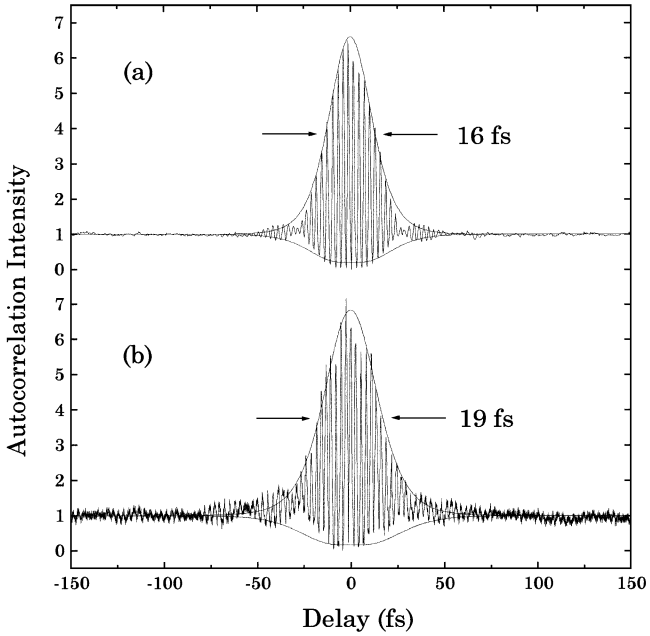

Fig. 8. (a) The oscillating curve is the collinear intensity autocorrelation trace of the input pulse of the pulse shaper. The intensity at sufficiently long delay is normalized to unity. The smooth curves are the envelopes of the best fit autocorrelation function of sech^2 pulses with a pulse width of 16 fs. (b) The oscillating curve is the cross-correlation of the input pulse and the output pulse of the pulse shaper with no modulation pattern on the SLM. The intensity at sufficiently long delay is normalized to unity. The smooth curves are the calculated envelopes of autocorrelation of 19 fs sech^2 pulses.

laser beam was split by a beam splitter, and one beam was directed to the pulse-shaping apparatus described above. The other beam was used as the reference in the cross-correlation measurements. The output beam of the pulse-shaping apparatus was combined with the reference beam collinearly by another beam splitter. The combined beam was focused on to a GaAsP photodiode (Hamamatsu G1116) using a concave mirror, and two-photon-induced photocurrent in the GaAsP photodiode was measured.[10] The path length of the reference beam could be scanned by a translation stage driven by a stepping motor, and could also be modulated by a piezoelectric actuator at about 1 kHz.

The output beam of the femtosecond Ti:sapphire laser was passed through a sequence of four silica prisms before it was incident into the cross-correlation measurement setup, and the group-velocity dispersion (GVD) of optical elements was compensated for. The input pulse waveform was characterized by a collinear intensity autocorrelator using the same beam splitter and the same GaAsP photodiode as those used in the cross-correlator. The autocorrelator was prepared separately from the cross-correlation setup. The autocorrelation of the input pulse obtained is shown in Fig. 8(a). By assuming a sech^2 pulse shape, the pulse width was obtained to be 16 fs.

Figure 8(b) shows the cross-correlation between the reference pulse and the output pulse of the pulse shaping apparatus with no modulation pattern on the SLM. The position of the grating on the output side in the pulse shaper was adjusted to minimize the width of the cross-correlation trace. The trace was slightly broadened from the autocorrelation of the unshaped pulse, and best fit by a theoretical autocorrelation trace of 19 fs pulses by assuming a sech^2 pulse shape. Broadening of the reference pulse is impossible since the beam passed through the same optical elements in the autocorrelator and in the cross-correlation measurement apparatus. Therefore, the broadening of the cross-correlation trace is attributed to the broadening of the pulses that passed through the pulse-shaping apparatus. The actual pulse width of the output pulse is estimated to be around 22 fs, although information on chirping of the output pulse is required to obtain an exact value of the pulse width. This slight broadening of the pulse that passed through the apparatus is probably due to the GVD in the SLM and the polarizer which was attached to the SLM. Although first-order GVD can be compensated for by adjusting the position of the grating, effects of higher order GVD cannot be eliminated.

The transmittance of the laser light through the SLM was measured as a function of the discrete level of the voltage applied to the SLM. Using the result of this measurement and the theoretical transmission coefficient shown in eq. (1), the applied voltage level was related to the birefringence parameter u, which was used in the SA calculation.

For measurements of the cross-correlation of shaped pulses, we modulated the reference path length by using the piezoelectric actuator attached to a mirror in the reference beam path, and lock-in detected the signal current. This technique ensured better quality of data, and eliminated the inevitably large background in the collinear cross-correlation signal with unbalanced inputs. The trace obtained in this measurement corresponds to a time derivative of the actual cross-correlation.

An example of shaped pulse waveforms observed by the path-length modulated collinear cross-correlation measurement is shown in Fig. 9(b). The modulation pattern of the SLM used is shown in Fig. 4, and it is expected that the generated pulse has the waveform shown in Fig. 3. The simulated cross-correlation trace obtained from the shaped waveform of Fig. 3 is shown in Fig. 9(a). A shaped pulse is observed at 126 fs, as designed in the positive time region. However, the peak height of the shaped pulse is not as large as expected. The origin of this disagreement is probably due to the inappropriate characterization of the transmission properties of light passing through the SLM. In the present study, the applied voltage dependence of the transmittance was mea-

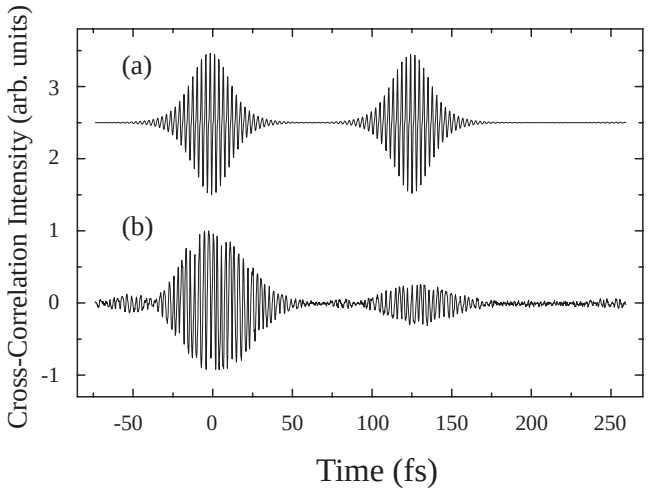

Fig. 9. (a) Simulated path-length modulated cross-correlation trace from the shaped waveform shown in Fig. 3. (b) Observed cross-correlation trace of the shaped waveform generated by the SLM modulation pattern shown in Fig. 4.

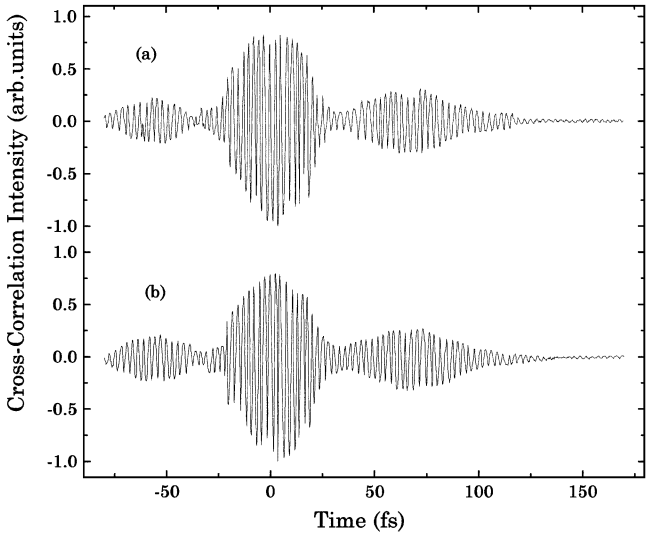

Fig. 10. Path-length modulated cross-correlation traces for two target waveforms with the same temporal position of the pulse at 63 fs in the positive time region, and a phase difference of π.

sured experimentally. The phase change, however, was estimated using the theoretical relation of the amplitude and the phase for a TN liquid-crystal panel with a twist angle of 90°. It was recently reported[11] that the twist angles of some TN liquid-crystal panels used in commercial visual instruments are considerably less than 90°. Full experimental characterization of the transmission properties of the SLM by interferometric measurement is now in progress, and preliminary results suggest a phase spectrum different from that estimated for a 90° twist angle. It is expected that a mask pattern obtained by a new SA calculation based on the experimentally obtained amplitude-phase relation will generate a waveform with a larger pulse height.

Figure 10 shows cross-correlation traces of two shaped waveforms. Here, not only the peak intensity but also the phase of the shaped pulse was controlled. For the SA calculation of the mask pattern which generates phase-sensitive waveforms, the cost function was modified from that shown in

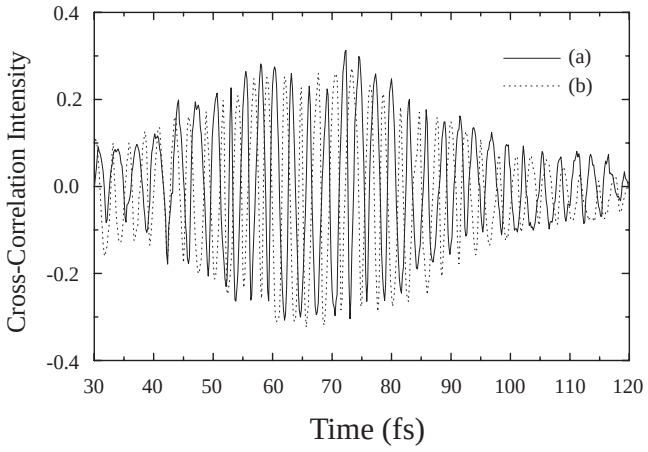

Fig. 11. Traces in Fig. 10 are expanded around the time region of the shaped pulse. It is clearly shown that the phases of the oscillations of the two traces are inverted from each other. Curves (a) (solid line) and (b) (dashed line) correspond to curves (a) and (b) in Fig. 10, respectively.

eq. (10). The peak intensities I_k ($k = 1 \ldots N$) defined in eq. (7) were divided into contributions of two mutually orthogonal phase components. The amplitude of the relevant mode in the resultant $2N$-dimensional space was maximized by the SA algorithm in the same manner as described above. The target waveforms of the two traces shown in Fig. 10 had a pulse peak at the same time of 63 fs, and the phases of the field oscillations at the peak time were inverted from each other. This phase inversion is clearly seen in Fig. 11, where the two traces in the 30–120 fs region are expanded. Little phase difference, however, between the two traces was observed in the time region around the time origin, where the unshaped pulse remained. The shaped pulses obtained by this phase-sensitive pulse-shaping technique can be applied to the phase-sensitive coherent control of dynamics in many kinds of materials.[12]

5. Conclusions

We theoretically and experimentally characterized the properties of a commercial TN liquid-crystal SLM with a large number of pixels. We developed the relevant mode extraction method for the calculation of mask patterns which can generate multiple pulse sequences with arbitrary relative amplitudes and phases. We succeeded experimentally in shaping femtosecond pulses at a desired time with a specific phase using a pulse-shaping apparatus implemented with a TN SLM. A smaller amplitude of the shaped pulse than expected indicates that the actual SLM modulation function differs from the one used in the calculation.

The shaped waveforms were observed by measuring the interferometric intensity cross-correlation. To our knowledge, this is the first direct experimental observation of the phase of output pulses of the pulse-shaping apparatus.

The peak around time zero in the shaped waveform is always present due to the limited possible phase change of the SLM modulation function. Removing this peak by spatial filtering using the coupling between the spatial and temporal profiles of the shaped waveforms[5] will be possible because of the large pixel number of the SLM.

Acknowledgements

This work was supported in part by a Grant-in-Aid for Scientific Research (C) from the Ministry of Education, Science, Sports and Culture.

1) D. H. Reitze, A. M. Weiner and D. E. Leaird: Appl. Phys. Lett. **61** (1992) 1260.
2) A. M. Weiner, S. Oudin, D. E. Leaird and D. H. Reitze: J. Opt. Soc. Am. B **10** (1993) 1112.
3) A. Efimov, C. Schaffer and D. H. Reitze: J. Opt. Soc. Am. B **12** (1995) 1968.
4) M. M. Wefer and K. A. Nelson: J. Opt. Soc. Am. B **12** (1995) 1343.
5) M. M. Wefer and K. A. Nelson: IEEE J. Quantum Electron. **32** (1996) 1.
6) R. M. Koehl, T. Hattori and K. A. Nelson: Opt. Commun. **157** (1998) 57.
7) C. H. Gooch and H. A. Tarry: J. Phys. D **8** (1975) 1575.
8) M. T. Asaki, C. -P. Huang, D. Garvey, J. Zhou, H. C. Kapteyn and M. M. Murnane: Opt. Lett. **18** (1993) 977.
9) See, for example, W. H. Press, S. A. Teukolsky, W. T. Vettering and B. P. Flannery: *Numerical Recipes* (Cambridge University Press, Cambridge, 1992), Chap. 10.
10) J. K. Ranka, A. L. Gaeta, A. Baltuska, M. S. Pshenichnikov and D. A. Wiersma: Opt. Lett. **22** (1997) 1344.
11) I. Moreno, N. Bennis, J. A. Davis and C. Ferreira: Opt. Commun. **158** (1998) 231.
12) A. P. Heberle, J. J. Baumberg and K. Köhler: Phys. Rev. Lett. **75** (1995) 2598.